JOURNAL OF MATERIALS SCIENCE 33 (1998) 4561–4568

Effect of silicon-ion implantation upon the corrosion properties of austenitic stainless steels

J. BASZKIEWICZ, J.A. KOZUBOWSKI, D. KRUPA, M. KAMIŃSKI
Department of Materials Science and Engineering, Warsaw University of Technology, Narbutta 85, 02–524 Warsaw, Poland
E-mail:

A. BARCZ
Institute of Electron Technology, Al. Lotników 46, 02-668 Warsaw, Poland

G. GAWLIK, J. JAGIELSKI
Institute of Electronics Materials Technology (IEMT), Wólczyńska 133, 01-919 Warsaw, Poland
E-mail: JBASZ@MEIL.PW.EDU.PL

The structure of the surface layers and the corrosion resistance of austenitic stainless steels after silicon-ion implantation, were examined. The implanted silicon doses were 1.5×10^{17}, 3×10^{17} and 4.5×10^{17} Si^+ cm^{-2}. Implantation with all these doses gave an amorphous surface layer. When samples implanted with 1.5×10^{17} Si^+ cm^{-2} were annealed at temperatures of 300 and 500 °C, their surface structure remained unchanged. After annealing at 650 °C, the amorphous layer vanished. It was determined how, in terms of corrosion resistance, the amount of implanted silicon, subsequent heat treatment and long time exposure, affect highly corrosion-resistant austenitic stainless steel (18/17/8) in comparison to the 316L austenitic stainless steel subjected to the same treatment. Corrosion examinations were carried out in 0.9% NaCl at a temperature of 37 °C. After silicon-ion implantation the corrosion resistance of the 316L steel increased while that of highly resistant (18/17/8) did not. The corrosion resistance of the investigated steels, both implanted and non-implanted, increased with the exposure time of the samples in the test environment. © *1998 Kluwer Academic Publishers*

1. Introduction

Implantation of appropriately chosen ions into the surface of metals mostly increases their corrosion resistance and improves their tribological properties. For example, silicon ions implanted into the surface of iron increase its corrosion resistance [1]. An increase in the wear resistance of 304 steel after the implantation with silicon ions was reported by Fayeulle *et al.* [2]. Baszkiewicz *et al.* [3] report on an increased corrosion resistance of alloy steels due to silicon implantation. Baszkiewicz *et al.* [3–6] also examined the three stainless steels: 430 (0.08C, 0.5Ti), 304L and 316 (0.4Ti), which were implanted with silicon doses of 0.5×10^{17}, 1×10^{17} and 1.5×10^{17} Si^+ cm^{-2} at a beam energy of 100 keV. It has been bound that the implantation results in a solid amorphous layer being formed on the steel surface.

When examined in hydrochloric acid, all the implanted steels exhibited an increased resistance to corrosion; in sodium chloride, an increased corrosion resistance was evident for 430 and 316 steels. The greatest increase of the corrosion resistance was observed at the highest silicon dose. Baszkiewicz *et al.* [6] discussed how the annealing affects the structure and corrosion resistance of 316 (0.4Ti) steel implanted with 1.5×10^{17} Si^+ cm^{-2}. After implantation, the samples were annealed at temperatures of 300 and 500 °C. The annealing at 300 °C had no effect upon the amorphous layer, whereas after annealing at 500 °C, a fine grained structure formed. The corrosion resistance was examined in non-aerated 0.1M HCl. The samples annealed at 300 °C exhibited an increased corrosion reistance, and those annealed at 500 °C a reduced one. The authors attributed this reduction of corrosion resistance to the crystallization of the surface layer during the annealing (the amorphous layer vanished). SIMS examinations of the chemical composition of the implanted samples after corrosion tests show that the concentrations of iron, chromium and nickel in the surface layer have decreased, whereas the concentrations of silicon and oxygen increased. The results obtained suggests that a surface silicon oxide layer, most probably SiO_2 has formed [7]. Perhaps it is this oxide layer that increases the corrosion resistance of silicon-implanted steel. Examination of 304 austenitic steel implanted with silicon were reported by Feyeulle *et al.* [2]. They used silicon ions of energy of 40 eV in the does from 5×10^{16} to 2×10^{17} Si^+

cm^{-2} and, with all the doses, obtained an amorphous layer; with the higher dose, Fe_3Si precipitates were additionally observed. The implantation increased the wear resistance of the steel examined.

The aim of the present study was to determine how, in terms of corrosion resistance, the amount of implanted silicon, subsequent heat treatment and long time exposure, affect highly corrosion resistant austenitic stainless steel (steel B Table I) and how it compares to the properties of 316L austenitic stainless steel subjected to the same treatment.

2. Experimental procedure

The chemical compositions of the steels examined are given in Table I. The steel designated as A is 316L steel, and steel B has no ASTM designation because it originates from an experimental melt. Test samples were prepared from the sheet by cutting discs 13 mm diameter and 3 mm thick. The surface of the samples were polished mechanically to a mirror finish and, then, electrochemically in a solution composed of 96% CH_3COOH, 4% H_2O and 200 g dm^{-3} CrO_3. The implantation with silicon ions was performed at the Department of Ionic Techniques, ITME, Warsaw, using a Balzers MPB-202RP implantator. The silicon ion doses were 1.5×10^{17}, 3×10^{17} and 4.5×10^{17} Si^+ cm^-. The ion-beam energy was 100 keV and the beam current ranged from 1–1.5 μA cm^{-2}. The temperature of the samples during the implantation did not exceed 70 °C

After the implantation, parts of the samples implanted with dose 1.5×10^{17} Si^+ cm^{-2} were annealed under vacuum at temperatures of 300, 500 and 650 °C for 1 h. Structural examination was made with a Philips EM300 transmission electron microscope (TEM). The test specimens were cut by the electric spark method and then thinned on the non-implanted surface until a perforation occured.

The chemical composition of the surface layers was identified by secondary ion spectrometry (SIMS). The chemical composition profiles were determined using an argon beam of energy of 4 keV. The scanned area was about 1 mm^2 and the material removal rate was about 0.15 nm s^{-1}. The samples examined by SIMS included samples in the starting state and implanted samples before and after the corrosion measurements. The resistance of corrosion of the samples was examined in the 0.9% NaCl environment at a temperature of 37 °C using two methods: the linear polarization method and the potentiodynamic method. The samples were exposed to the test conditions for 24 h and then their corrosion potential was measured. After this measurement, the samples were polarized in the anodic direction starting from -600 mV up to the moment when the current density reached 5 mA cm^{-2}. The potential variation rate was 1000 mV h^{-1}. The reference electrode was a saturated calomel electrode. Prior to the electrochemical examinations, part of the samples were exposed to the test conditions for 1200 h. During the long-term exposures, the measured pH of the solution was 6.6 ± 0.3 pH units and varied only slightly during the exposure. After the polarization, the samples were examined using an optical microscope and a scanning electron microscope (SEM).

3. Results

3.1 TEM results

The results of the structural examinations are shown in Figs 1–5. Fig. 1 shows the microstructure of non-implanted steel A (316L). We can see large (of the order of 10 μm) grains of austenite, often twinned, with dislocations occurring within the grains and at the grain boundaries.

The microstructure and the diffraction pattern of a sample of steel A implanted with a dose of 1.5×10^{17} Si^+ cm^{-2} are shown in Fig. 2. In Fig. 2a we can see dark dots about 3 nm in size, which can be interpreted as coherently dispersing nanocrystals. The diffraction pattern (Fig. 2b) contains rings A and B which are due to the diffraction on an amorphous phase. Ring B (the second in the sequence) is very weak which suggests that the short-range ordering is greatly varied. Ring C results from the double diffraction on the amorphous phase and the matrix. The reflections from the substrate (austenite) contain satellites, which provides evidence that plate-like cohorent precipitates are present. Fig. 3 shows the structure and the diffraction pattern of a sample of steel A implanted with a dose of 3×10^{17} Si^+ cm^{-2}. In Fig. 3a we can see a polycrystalline layer with crystallites greatly varying in size: from several to 200 nm. The diffraction pattern of this layer

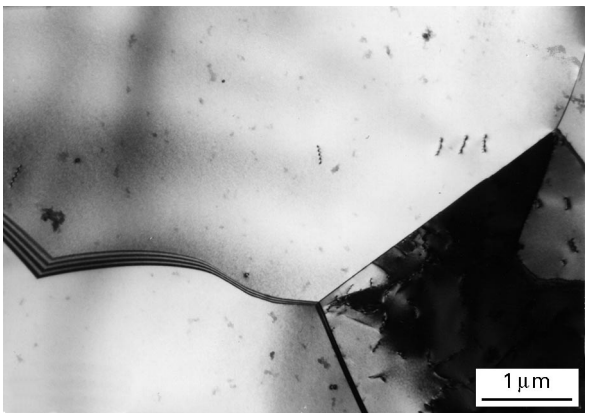

Figure 1 Microstructure of steel A (316L).

TABLE I Chemical composition wt % of investigated stainless steels (balance Fe)

Steel	C	P	S	Mn	Si	Cr	Ni	Mo	Ti
A	0.02	0.02	0.003	1.84	0.24	17.3	13.9	2.83	0.11
B	0.05	0.019	0.016	1.51	0.56	18.1	16.6	7.9	0.51

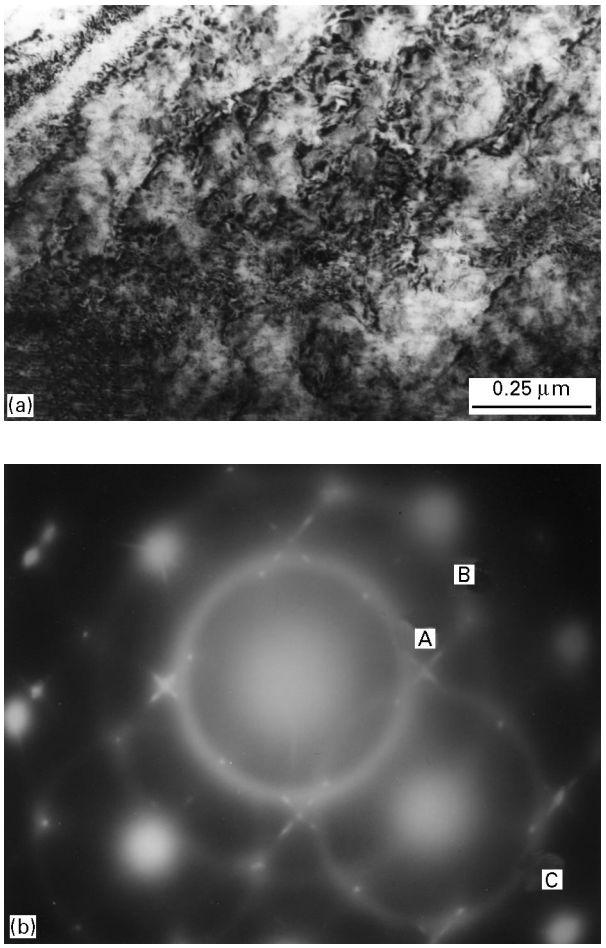

Figure 2 Microstructure (a) and diffraction pattern (b) of silicon implant steel A (316L) for the dose of 1.5×10^{17} Si^+ cm^{-2}.

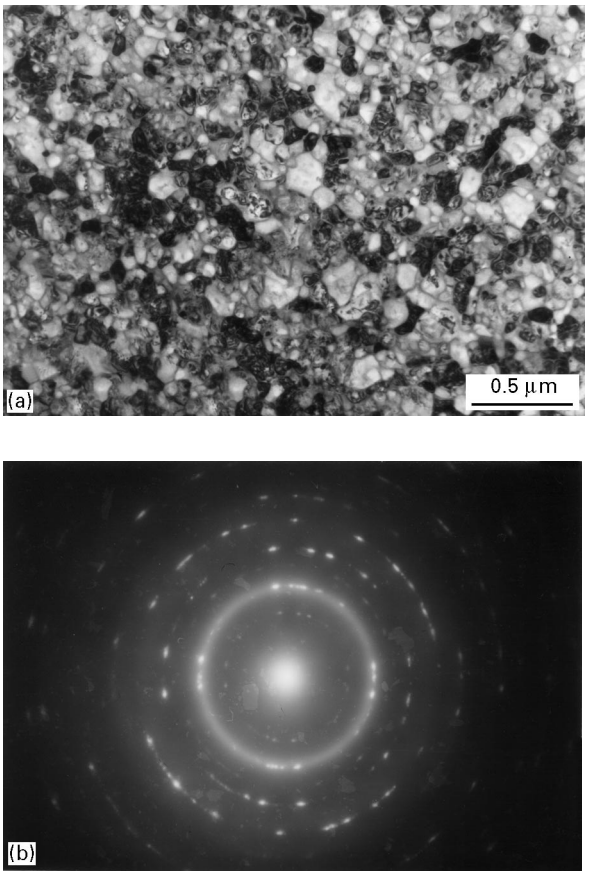

Figure 3 Microstructure (a) and diffraction pattern (b) of silicon implanted steel A (316L) for the dose of 3×10^{17} Si^+ cm^{-2}.

(Fig. 3b) is consistent with martensite while a blurred continuous ring is due to an amorphous phase. There are also a few reflections (inside the first ring) from an unidentified silicide phase. The structure and diffraction patterns of the samples implanted with 4.5×10^{17} Si^+ cm^{-2} are similar to those obtained for a dose of 3×10^7 Si^+ cm^{-2} and hence we infer that the structural changes due to these two doses are similar. The effect of annealing upon the structure of the surface layer implanted on steel A samples with a dose of 1.5×10^{17} Si^+ cm^{-2} is illustrated in Figs 4 and 5. The annealing was carried out at temperatures of 300, 500 and 650 °C. Because the structural changes after annealing at 300 and 500 °C were similar, Fig. 4a shows only the results obtained at 500 °C, nanocrystallites, 3 nm in size, of an unidentified silicide phase are visible. The diffraction pattern indicates the presence of an amorphous phase. The second ring, more pronounced, is evidence that this phase has undergone ordering. After annealing at 650 °C, the amorphous phase vanished (Fig. 5). Fig. 5a shows a polycrystalline layer composed of grains of various sizes. The average grain size is 200 nm. The size of the "grey" relatively large recrystallized grains is of the order of 1 μm. From the diffraction pattern (Fig. 5b) the structure can be identified as martensite and an unidentified silicide (or silicides) of low symmetry and lattice parameter close to 0.64 nm. No signs of the presence of the amorphous layer were found. The structure shown in Fig. 5a consists of martensite grains mixed with silicide grains. Structural examinations of samples of silicon-implanted steel B indicates the presence of an amorphous layer, as an steel B. In contrast to steel A, no martensitic phase was observed after the implantation. The amorphous layer does not crystallize during annealing at 500 °C, but only at 650 °C when the crystallization is accompanied by the formation of martensite.

3.2. SIMS examinations

SIMS silicon concentration profiles of the surface layer implanted with a dose of 1.5×10^{17} S^+ cm^{-2}, i.e. the distribution of the implanted silicon concentration with the distance from the surface depending on the annealing temperature, are shown in Fig. 6. The annealing at 300 and 500 °C leads to a significant diffusion of silicon; the extent of the relocation of the silicon atoms suggests the grain-boundary diffusion to be dominant process.

3.3. Corrosion resistance

3.3.1. Effect of the silicon dose and the preliminary exposure time on the corrosion resistance

The results of examinations of the corrosion resistance depending on the implanted silicon dose are given in

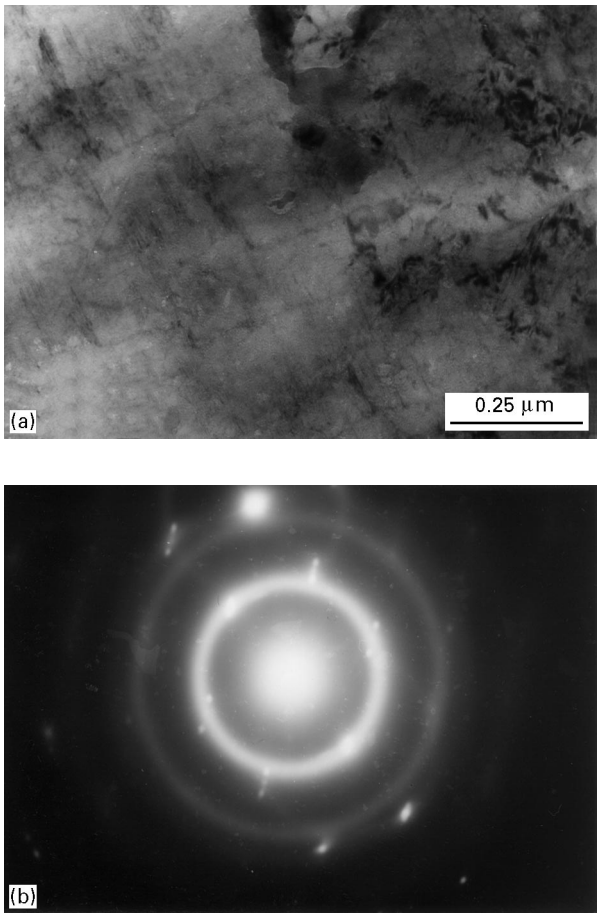

Figure 4 Microstructure (a) and diffraction pattern (b) of silicon implanted steel A (316L) for the dose of 1.15×10^{17} Si^{+} cm^{-2}. After implantation, specimens were annealed 1 h at 500 °C.

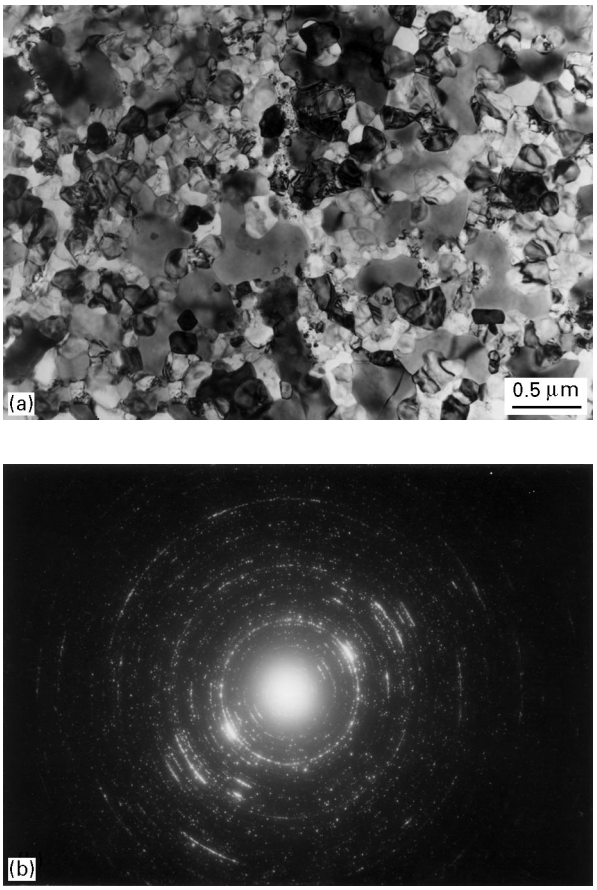

Figure 5 Microstructure (a) and diffraction pattern (b) of silicon implanted steel A (316L) for the dose of 1.5×10^{17} Si^{+} cm^{-2}. After implantation specimens were annealed 1 h at 650 °C.

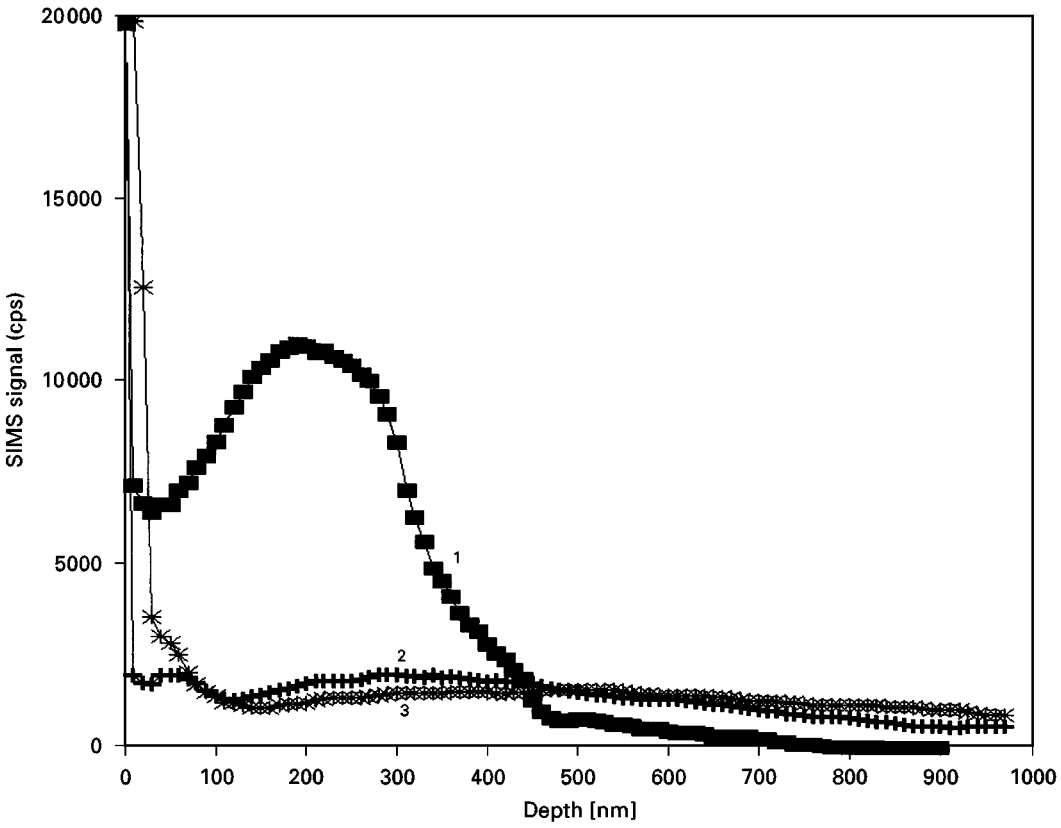

Figure 6 Silicon concentration depth profiles steel A (316L). Specimen implanted with a 1.5×10^{17} Si^{+} cm^{-2} dose. 1, Non-annealed; 2, annealed 300 °C 1 h; 3, annelated 500 °C 1 h.

Table II and in Figs 7–12. The values of the polarization resistance R_p, after a 24 h exposure show that, after the silicon implantation, the corrosion resistance of both kinds of steel increases. For an increased

TABLE II Polarization resistance of investigated stainless steels implanted with silicon ions for 24 or 1200 h exposure

Steel	Dose Si (10^{17} Si^+ Cm^{-2})	Polarization resistance, R_p ($M\Omega\,cm^{-2}$)	
		24	1200
A	Non-implanted	1	3
	1.5	3	6
	3	17	12
	4.5	14	30
B	Non-implanted	2	8
	1.5	3.5	16
	3	3	20
	4.5	3	35

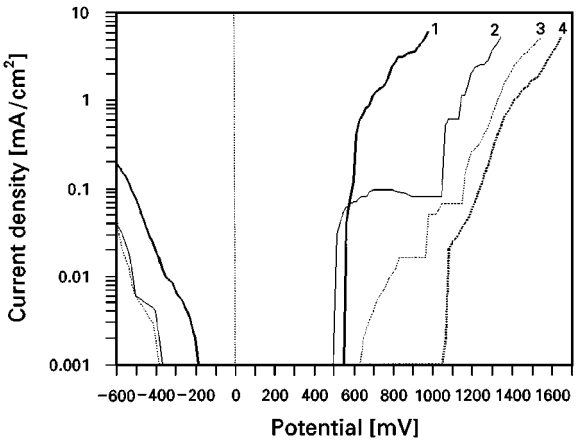

Figure 9 The anodic polarization curves measured for the A (316L) steel in a solution of 0.9% NaCl after 1200 h exposure. 1, Non-implanted specimen; 2, specimen implanted with a 1.5×10^{17} Si^+ cm^{-2} dose; 3, specimen implanted with a 3×10^{17} Si^+ cm^{-2} dose; 4, specimen implanted with a 4.5×10^{17} Si^+ cm^{-2} dose.

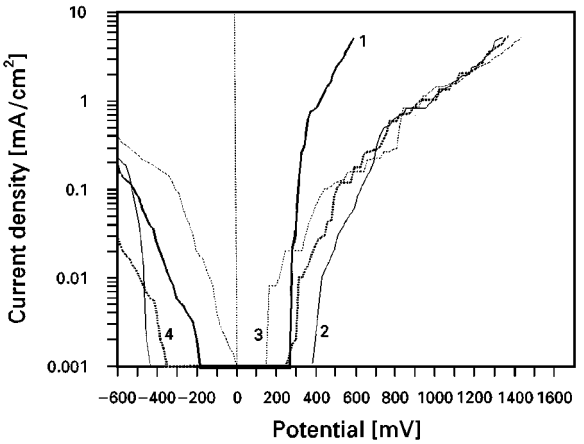

Figure 7 The anodic polarization curves meausred for the A steel in a solution of 0.9% NaCl after 24 h exposure. 1, Non-implanted specimen; 2, specimen implanted with a 1.5×10^{17} Si^+ cm^{-2} dose; 3, specimen implanted with a 3×10^{17} Si^+ cm^{-2} dose; 4, specimen implanted with a 4.5×10^{17} Si^+ cm^{-2} dose.

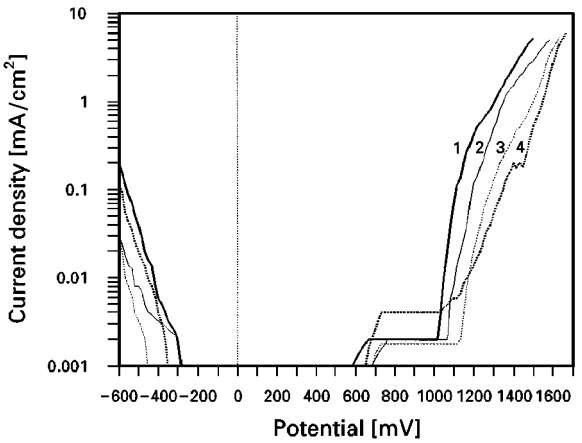

Figure 10 The anodic polarization curves measured for the B steel in a solution of 0.9% NaCl after 1200 h exposure. 1, Non-implanted specimen; 2, specimen implanted with a 1.5×10^{17} Si^+ cm^{-2} dose; 3, specimen implanted with a 3×10^{17} Si^+ cm^{-2} dose; 4, specimen implanted with a 4.5×10^{17} Si^+ cm^{-2} dose.

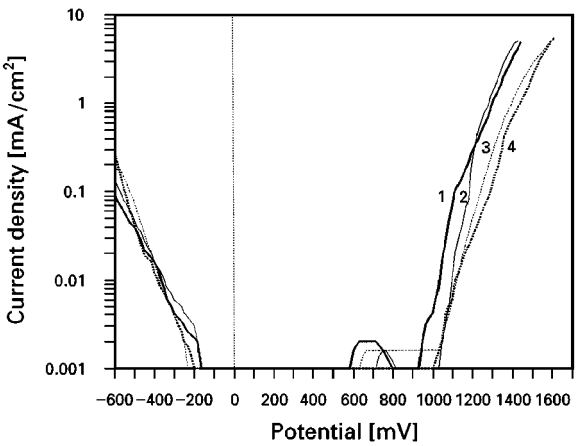

Figure 8 The anodic polarization curves measured for the B steel in a solution of 0.9% NaCl after 24 h exposure. 1, Non-implanted specimen; 2, specimen implanted with a 1.5×10^{17} Si^+ cm^{-2} dose; 3, specimen implanted with a 3×10^{17} Si^+ cm^{-2} dose; 4, specimen implanted with a 4.5×10^{17} Si^+ cm^{-2} dose.

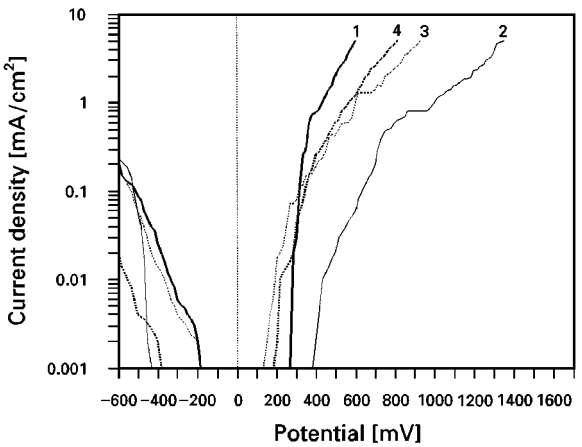

Figure 11 The anodic polarization curves measured for the A (316L) steel in a solution of 0.9% NaCl after 24 h exposure. 1, Non-implanted specimen; 2, specimen implanted with a 1.5×10^{17} Si^+ cm^{-2} dose; 3, specimen implanted with a 1.5×10^{17} Si^+ h^{-1}, annealed 1 h at 300 °C; 3, specimen implanted with a 1.5×10^{17} Si^+ h^{-1}, annealed 1 h at 500 °C.

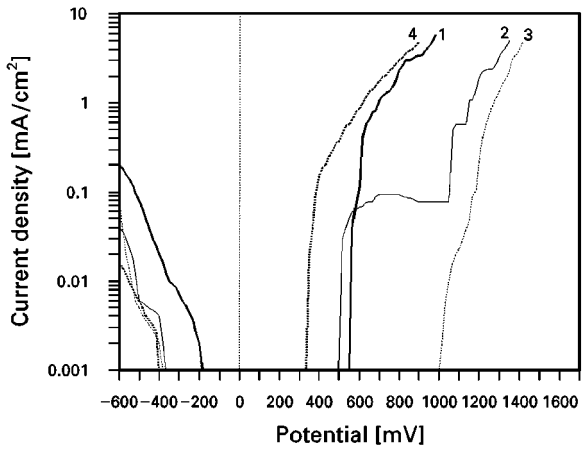

Figure 12 The anodic polarization curves measured for the A (316L) steel in a solution of 0.9% NaCl after 1200 h exposure. 1, Non-implanted specimen; 2, specimen implanted with a 1.5×10^{17} Si^+ cm^{-2} dose; 3, specimen implanted with a 1.5×10^{17} Si^+ h^{-1} annealed 1 h at 300 °C; 3, specimen implanted with a 1.5×10^{17} Si^+ h^{-1}, annealed 1 h at 500° C.

silicon dose, R_p increases in steel A and remains unchanged in steel B. When preliminary exposure time was increased to 1200 h, the polarization resistance of both the non-implanted and implanted samples increased. With both kinds of steel, the polarization resistance increases with increasing silicon dose. This was particularly pronounced in steel B. The polarization curves shown in Fig. 7 indicate that, after 24 h exposure, it is only the 1.5×10^{17} Si^+ cm^{-2} does which improves the corrosion resistance. A further increase of the dose has no effect upon the corrosion resistance. After the silicon implantation, the corrosion pits develop more slowly (the slope of the polarization curve is not as steep as that obtained for non-implanted steel).

In steel B after the 24 h exposure (Fig. 8), the effect of implantation manifests in a slight shift of the polarization curves towards more positive potentials and a reduction of the current magnitudes within the transpassive region. This reduction is the greatest in the samples implanted with the highest silicon dose.

In steel A, an increases of the preliminary (before the measurement) exposure time to 1200 h results in the polarization curves being changed in shape and shifted towards the positive potential values (Fig. 9). This was most pronounced in the samples implanted with the highest silicon dose.

In steel B, the same increase of the preliminary exposure time does not affect the shape of the polarization curves. The only effect in this steel was an increase of the currents of the transpassive state (compared with these currents measured in the samples exposed for 24 h).

3.3.2. Effect of the post-implantation annealing on the corrosion resistance

This effect was examined in samples implanted with a dose of 1.5×10^{17} Si^+ cm^{-2}. The results are shown in Table III and in Figs 11 and 12.

TABLE III Polarization resistance of investigated stainless steels implanted with 1.5×10^{17} Si^+ cm^{-2} and annealed after implantation, for 24 or 1200 h exposure

Steel	Annealing temperature (°C)	Polarization resistance, R_p ($M\Omega\,cm^{-2}$)	
		24	1200
A	Non-annealed	3	6
	300	–	11
	500	–	4
B	Non-annealed	3.5	16
	300	1	1
	300	6	32

In steel A, after annealing at 300 °C and preliminary exposure for 1200 h, the polarization resistance R_p increases, whereas after annealing at 500 °C it decreases compared to that measured in non-annealed samples. After exposure for 24 h, the post-implantation annealing causes the polarization curves of this steel (Fig. 10) to shift towards the negative potentials. When the samples are exposed for 1200 h (Fig. 12), the corrosion resistance increases after annealing at 300 °C and decreases after annealing at 500 °C.

In steel B, the shape of the polarization curves does not change after the post-implantation annealing. In non-implanted steel A, the polarization curves also remain almost unchanged irrespective of whether the samples were annealed at 300 or at 500 °C.

3.4. SEM examinations

During corrosion examinations, the non-implanted samples underwent pitting corrosion typical of austenitic stainless steel in the environment of chlorides. On the surface of the implanted samples, a relatively great number of minute pits occurred (Fig. 13). The pits had spherical or nearly spherical shapes and were covered with residues of the implanted layer. Pits of similar shapes were observed on the surface of molybdenum-implanted UNSS30100 steel by Ives *et al.* [8]. They found that the pits occurred in the places where the passive layer had been damaged, and developed as subsurface pits. Fig. 13a–d show the successive stages of the development of the pits that occur on the surface of implanted samples. The pits may originate at "subsurface micropits" (Fig. 13a, b, e). The fact that the pits have spherical shapes may perhaps be associated with the presence of a nanocrystalline austenitic layer beneath the amorphous layer (Fig. 13e). An initiated pit grows under the amorphous layer as a subsurface pit (Fig. 13b,c) within which the nanocrystalline austenite layer is dissolved. Because in this layer, no preferred direction of the dissolution exists, the growing pit takes the around shape. If the pits grow under the implanted layer, which is not dissolved so readily, the anodic processes are slowed (compared to those proceeding in non-implanted samples), which is manifested in the slower increase of the anodic current density (Fig. 7) or in the appearance of flat portion in the anodic polarization curves (Figs 9 and

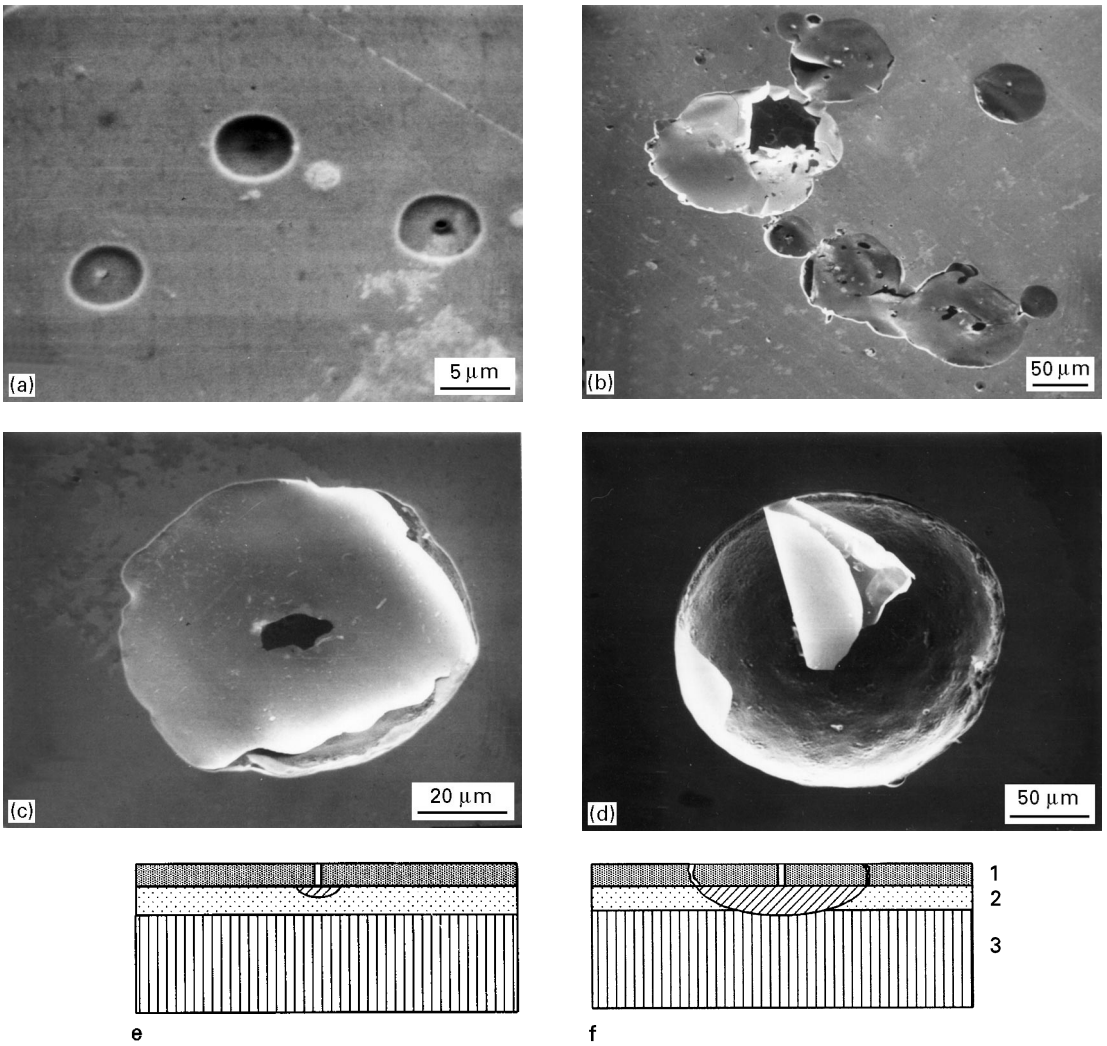

Figure 13 The appearance of surfaces of specimen implanted with a 3×10^{17} Si^+ cm^{-2} dose after anodic polarization. (a.c.d) Steel A, (b) steel B. (e.f.) Schematic development of pits under the implanted layer; 1, amorphous layer; 2, nanocrystaline layer; 3, unchanged steel structure (vertical scale exaggerated).

12). It is only after the pit achieves appropriate dimensions, when the slow-dissolving surface layer cracks, most often at the edge of the pit (Fig. 13b,c), and breaks off, which facilitates mass transfer and increases the anodic current density. The initial stages of the growth of a corrosion pit are shown in Fig. 13e and f.

4. Discussion

In the present experiments, we obtained an amorphous surface layer on both the implanted stainless steel examined and for all the silicon dose employed. The results obtained are in agreement with data reported in the literature [2, 6, 9, 10]. In both steels, the amorphous phase crystallized after annealing at a temperature of 650 °C. This is not consistent with the results given elsewhere [6, 9]. Baszkiewicz *et al.* [6] observed the crystallization of the amorphous phase after annealing at 500 °C. Rausenbach and Hohmuth [9], who implanted silicon ions into iron, reported that the temperature of crystallization of the amorphous phase ranged from 380–425 °C. In our experiments the crystallization occurred between 500 and 650 °C. It is difficult to explain unequivocally these differences. With doses above 1.5×10^{17} Si^+ cm^{-2}, we identified martensite in the implanted surface layer of steel A. Martensite forms as a result of the internal stresses induced during the implantation [10, 11]. When implanting silicon, the fact that silicon added to iron widens the range of occurrence of ferrite may also be important. In steel B, no martensite was found, which may perhaps be attributed to the higher carbon and nickel contents in steel B as compared with steel A – carbon and nickel increases the stability of the austenitic structure.

Martensite forms in steel B during annealing at 6750 °C and this may be due to silicon behaving as an alloying additive. The formation of martensite during the implantation is disadvantageous from the point of view of medical applications of silicon-implanted steels (implants) [12]. In the present experiments we did not identify the type of silicide found in the surface layer and we did not confirm the presence of Fe_3Si reported by Fayeulle *et al.* [2]. The effect of implanted silicon ions upon the corrosion resistance of the steels examined is varied. After a short-term preliminary exposure, the polarization resistance increases considerably in steel A and only slightly in steel B (Table II). After the implantation, the surface layer of both

steels was amorphous, but this did not affect the corrosion resistance of steel B: the polarization resistance and the course of the polarization curves showed only slight changes (Fig. 10). Steel B is more resistant to pitting corrosion than steel A – the potentials at which pits occur are here higher. The increase of the polarization resistance, indicating that the corrosion current decrease, is associated with the changes in the surface structure: the amorphization of the surface and hence the vanishing of the grain boundaries, and also the effects of the ion sputtering which accompanies the implantation. Silicon improves the resistance to corrosion, especially in the presence of molybdenum [13, 14]. It also increases the corrosion resistance of metallic glasses [15]. The advantageous effect of silicon may perhaps result not only from its making the surface amorphous but also from its acting as an alloying additive that takes part in the formation of the passive layer. On the other hand, martensite and the polycrystalline layer (Fig. 3a) that appear in the surface layer after implantation with 3×10^{17} and 4.5×10^{17} Si^+ cm^{-2} do not reduce the polarization resistance; however, they do affect adversely the course of the anodic polarization curves (Fig. 7).

A prolonged exposure time leads to an increase of the corrosion resistance in both the steels, which can primarily be inferred from the increased polarization resistance. This can be attributed to the oxide layer becoming thicker and to the concentrations of the constituent elements of the surface layer being changed [16]. In the present study we have not defined the reasons for this increase of the corrosion resistance. If the implanted samples are subected to annealing at temperatures of 300 and 500 °C, their corrosion resistance changes. This effect is more pronounced in steel A, where, after an exposure for 24 h prior to the measurement, the corrosion resistance decreases (Fig. 11). This can be explained by the ordering of the amorphous layer (Fig. 4) or by a decrease of the silicon concentration in the surface layer (Fig. 6). Samples exposed for 1200 h before the measurement showed an increase of the corrosion resistance when annealed at 300 °C and a decrease when annealed at 500 °C. These results originate from two effects: the increase of the corrosion resistance due to the long-term exposure, which predominates in samples annealed at 300 °C, and the decrease of this resistance due to the ordering of the amorphous phase or to a reduction of the silicon concentration near the surface, which predominates in samples annealed at 500 °C. In steel B, the annealing only affects the values of the polarization resistance.

5. Conclusions

1. As a result of the silicon-ion implantation of the steels examined, an amorphous layer forms on their surface, and silicide precipitates, coherent with the basic lattice, are formed. After annealing at a temperature of 650 °C for 1 h, the amorphous layer vanishes.
2. Silicon-ion implantation of steel A (316L) using a dose above 1.5×10^{17} Si^+ cm^{-2} leads to the formation of martensite.
3. After the silicon-ion implantation, the corrosion resistance of the 316L steel increaced, while that of highly resistant steel B did not.
4. Long-term exposures in the test environment increase the corrosion resistance of the steels, both implanted and non-implanted. In those implanted, the increase of the corrosion resistance is more pronounced.
5. The amorphous layer formed on the surface of high alloy steel (B) does not affect the course of the anodic polarization curves is an essential manner.

Acknowledgement

This work was supported by the Polish Committee for Scientific Research (KBN) through research grant 3 P407 051 04.

References

1. MASAYA IVAKI, *CRC Crit. Rev. Solid State Mater. Sci.* **15**(5) (1989) 473.
2. S. FAYEULLE, D. TREHEUX and P. GUIRALDENQ, *Wear* **122** (1988) 255.
3. J. BASZKIEWICZ, M. KAMIŃSKI, A. PODGÓRSKI, J. JAGIELSKI and G. GAWLIK, *Corr. Sci.* **33** (1992) 815.
4. J. BASZKIEWICZ, M. KAMIŃSKI, *Ochrona przed korozja* **1991**(5) (1991) 102.
5. *Idem. Inzy. Mater.* **1991**(5) (1991) 114.
6. J. BASZKIEWICZ, M. KAMIŃSKI, D. KRUPA, J. KOZUBOWSKI, E. JEZIERSKA, G. GAWLIK, J. JAGIELSKI and A. J. BARCZ, "Materialy IV Krajowej Konferencji Korozyjnej Korozjas'93" (IChF PAN, Warszawa, 1993) p. 317.
7. A. J. BARCZ, M. BARTUR, T. BANWELL and M-A. NICOLET, *Electrochem. Soc.* **32** (1985) 2313.
8. M. B. IVES, U. G. AKANO, Y. C. LU, GUO RUIJIN and S. C. SRIVASTAVA, *Corr. Sci.* **31** (1990) 367.
9. B. RAUSCHENBACH and K. HOHMUTH, *Phys. Status Solidi A* **72** (1982) 667.
10. N. HAYASHI, E. JOHNSON, A. JOHANSEN, L. SARHOLT-KRISTENSEN and I. SAKAMOTO, Report No. 86-4 ISSN 0106-7222 H.C. Orsted Institute (1986).
11. R. LEUTENECKER, G. WAGNER, T. LOUIS, U. GONSER, L. LUZMAN and A. MOLINARI, *Mater. Sci. Eng.* **A115** (1989) 229.
12. J. MARCINAK, "Biomaterialy w chirurgii kostnej" (Wydawnictwo Politechniki Ślaskiej, Gliwice, 1992).
13. M. FONTANA and N. GREEN, "Corrosion Engineering", (McGraw-Hill, New York, 1978).
14. A. SEDRIKS, *Corr-NACE* **7** (1986) 376.
15. M. JANIK-CZACHOR, *Corr. Sci.* **31** (1990) 325.
16. R. DEVAUX, D. VOUANGNER, A. M. DEBEC-DELIEVRE and C. DURET-THUAL, *ibid.* **36** (1994) 171.

Received 24 November 1997
and accepted 15 May 1998